Supporting Information for

Slingshot homolog-1-mediated Nrf2 sequestration tips the balance from neuroprotection to neurodegeneration in Alzheimer's disease

Sara Cazzaro[1,5], Jung-A A. Woo[1], Xinming Wang[1], Tian Liu[1], Shanon Rego[5], Teresa Kee[1,5], Yeojung Koh[1,2,4], Edwin Vázquez-Rosa[2,4], Andrew A. Pieper[2,3,4,6,7,8], and David E. Kang[1,9,#]

[1]Department of Pathology, [2]Department of Psychiatry, [3]Department of Neuroscience, [4]Institute for Transformative Molecular Medicine, Case Western Reserve University, School of Medicine, Cleveland, OH, USA; [5]Department of Molecular Medicine, USF Health College of Medicine, Tampa, FL, USA; [6]Translational Therapeutics Core of Cleveland Alzheimer's Disease Research Center, [7]Geriatric Psychiatry, GRECC, Louis Stokes Cleveland VA Medical Center, [8]Brain Health Medicines Center, Harrington Discovery Institute, [9]Louis Stokes Cleveland VA Medical Center, Cleveland, OH, USA

[#]Correspondence: David E. Kang (dek94@case.edu)

Supplemental Text

SSH1-mediated suppression of Nrf2 is only moderately affected by endogenous p62

As SSH1 increased Keap1-Nrf2 interaction by sequestering p62 and reducing p62-Keap1 interaction, we determined whether SSH1-mediated suppression of nuclear Nrf2 is influenced by the presence of endogenous p62. As anticipated, $NaAsO_2$ treatment significantly increased endogenous nuclear Nrf2, and RNAi-mediated p62 knockdown significantly diminished nuclear Nrf2 levels at steady-state and after $NaAsO_2$ treatment (Figures S2K-S2M). Despite the changes by p62 siRNA, the magnitude of nuclear Nrf2 suppression by SSH1 overexpression was similar in the presence or absence of p62 siRNA at steady-state (Figures S2K-S2L). Moreover, SSH1 significantly reduced endogenous nuclear Nrf2 levels even with p62 siRNA and $NaAsO_2$ treatment, although the magnitude of nuclear Nrf2 suppression by SSH1 was notably moderated under this condition (Figures S2K-S2L). In addition to nuclear Nrf2 levels, we also examined Nrf2/ARE reporter activity in similar experiments. SSH1 overexpression significantly and strongly reduced Nrf2/ARE reporter activity in all conditions, regardless of $NaAsO_2$ treatment or p62 siRNA (Figures S2N-S2O), indicating that the ability of SSH1 to suppress nuclear Nrf2 signaling overall is only moderately affected by p62 knockdown.

SSH1-mediated Nrf2 suppression is distinct and separable from its actions on p62-mediated autophagy and cofilin activation

The N-terminal region of SSH1 1-461 (SSH1ΔC) containing the cofilin binding site and the catalytic domain (Figure S4A) is sufficient to dephosphorylate and activate cofilin as effectively as full-length SSH1 (1) but does not alter p62-mediated autophagy flux (2). The C-terminal half of SSH1 309-1049 (SSH1ΔN) containing the p62 binding site and the catalytic domain (Figures S4A) is sufficient to dephosphorylate p62 at pSer403 and inhibit p62-mediated autophagy flux as

effectively as full-length SSH1 but does not activate cofilin (2). Moreover, the catalytic phosphatase activity of SSH1 is required for both of these activities, in contrast to SSH1-mediated Nrf2 suppression. Hence, we further tested if SSH1ΔN and/or SSH1ΔC exhibits preferential activity on Nrf2 inhibition compared to full-length SSH1. In Nrf2/ARE reporter assays with H_2O_2 treatment, both SSH1ΔC and SSH1ΔN significantly reduced Nrf2-responsive reporter activity as measured by the ratio GFP/BFP fluorescence (Figures S4B-S4C). However, full-length SSH1 was significantly more effective than either deletion mutant in suppressing Nrf2/ARE reporter activity (Figures S4B-S4C). Moreover, whereas full-length SSH1 significantly blocked Nrf2-induced HMOX1 expression, SSH1ΔN and SSH1ΔC failed to do so (Figure S4D-S4E). Full-length SSH1 effectively bound Nrf2 (Figures S4F-S4G; Figure S4H, negative controls) and sequestered Nrf2 to the cytoskeletal fraction (Figures S4I-S4J). By contrast, neither SSH1ΔN nor SSH1ΔC were competent in these measures, corresponding to the more robust presence of full-length SSH1 with the cytoskeleton than either deletion mutant (Figure S4I-S4J).

Phosphorylation of p62 at Ser349 enhances its binding to Keap1 and suppresses Keap1-Nrf2 interaction (3), whereas p62 phosphorylation at Ser403 activates ubiquitinated cargo binding and autophagy flux (4-8). Notably, SSH1 fails to inhibit p62-mediated autophagy when the p62-Ser403 phosphorylation site is mutated to Ala or Glu (2). Hence, we tested whether SSH1 can inhibit p62-Keap1 binding in p62 harboring mutations at Ser349 or Ser403 phosphorylation sites. In WT GFP-p62 transfected cells, we detected robust p62-Keap1 interaction, which was significantly suppressed by SSH1 (Figures S4K-S4M; Figure S4L, negative controls). As expected, GFP-p62-S349A showed reduced interaction with Keap1 compared to WT GFP-p62. However, SSH1 failed to suppress p62-S349A association with Keap1 (Figures S4K-S4M), indicating the SSH1 preferentially inhibits pS349-p62/Keap1 interaction. We also observed strong p62-Keap1 interaction when transfected with GFP-p62-S403A or GFP-p62-S403E, and SSH1 effectively suppressed both p62-S403A or p62-S403E interactions with Keap1 (Figures S4N-

S4O). These results therefore indicate that SSH1-mediated suppression of Nrf2 signaling is distinct and separable from its activities on p62-mediated autophagy or cofilin activation.

Supplemental Methods

Chemicals and reagents

15-Deoxy-Δ12,14-prostaglandin J2 (Sigma-Aldrich, D8440), CDDO Methyl Ester (Sigma-Aldrich, SMB00376), sodium arsenite ($NaAsO_2$, Sigma-Aldrich, S7400), H_2O_2 (EMD Millipore, 386790), Tris-HCl: Tris (Thermo Fisher Scientific, BP152-10) / HCl (Fisher Chemical, A481-212), KCl (Sigma-Aldrich, 60128), $MgCl_2$ (Sigma-Aldrich, M9272), ATP (Thermo Scientific, R0441), DL-1,4-Dithiothreitol (DTT) (Acros Organics, 116558-0050), His-Nrf2 recombinant protein (MyBiosource, MBS205893), His-GST-Keap1 recombinant protein (SinoBiological, 11981-H20B), GST-SSH1 recombinant protein (Fisher Scientific, 89-963-276), and agarose-bound anti-rabbit beads (American Qualex, G1360B) were purchased from the indicated sources.

Mice

Previously described tau^{P301S} transgenic mice (PS19) (9) were obtained from Jackson Laboratories (B6; C3-Tg (Prnp-MAPT*P301S) PS19Vle/J, JAX: 008169). Genomic DNA isolated from tail snips was used for genotyping by PCR with the following primers: forward primer: 5' GGGGACACGTCTCCA 3', reverse primer: 5' TCCCCCAGCCTAGACCACGAG 3'.

Previously described $APP^{swe}/PS1^{dE9}$ transgenic mice (10) were obtained from Jackson Laboratories (B6;C3-Tg(APPswe,PSEN1dE9)85Dbo/Mmjax, JAX: 034829). Genomic DNA isolated from tail snips was used for genotyping by PCR with the following primers: forward primer: 5' CTGACCACTCGACCAGGTTCTGGGT 3', and reverse primer: 5' GTGGATAACCCCTCCCCCAGCCTAGAC 3'.

Ssh1$^{-/-}$ mice (TF3256) were generated by Lexicon Pharmaceuticals by gene trap insertion into intron 2 of *Ssh1* (11). Genomic DNA isolated from tail snips was used for genotyping by PCR with the following primers: TF3256 forward primer: 5' CGTAACTCTAGTTTATATGACCTGACACC 3', TF3256 reverse primer: 5'

TAGGCATATAGCTAGACTTCAGATGG 3', and LTR-2 primer: 5' AAATGGCGTTACTTAAGCTAGCTTGC 3'

Ssh1$^{-/-}$ mice were crossed with tau^{P301S} transgenic mice to generate tau^{P301S};*Ssh1*$^{-/-}$ mice. All mice were maintained in the C57BL/6 background for at least three generations prior to breeding. Water and food were supplied ad libitum with 12 h light/dark cycle under standard vivarium conditions. All experimental procedures on mice were approved by the IACUC.

Human brain tissue

Paraformaldehyde-fixed floating frontal cortex tissues were obtained from the Alzheimer's Disease Research Center at Emory University (Drs. Levey and Gearing). The primary neuropathologic diagnosis confirms AD and FTLD-tau patients (12). PMI, age at onset, duration of illness, age at death, *APOE* genotype, race, and gender are summarized in Figure S5A.

Real-time PCR

HEK293T cells were transfected with vector control or myc-Nrf2 and vector control or Flag-SSH1. Cells were harvested with 250µl trizol (Ambion, 15596026). After adding 62.5µl chloroform, samples were centrifuged at 13,000 RPM for 20 minutes at 4°C. RNA was isolated and purified with Monarch total RNA miniprep kit (New England Biolabs, T2010S) and then subjected to real-time PCR analysis using Brilliant III SYBR Green qRT-PCR Mix (Agilent Technologies, 600886). The comparative threshold cycle (Ct) value was measured on the CFX96 Touch Real-Time PCR Detection System (Bio-Rad) and used to calculate the amplification factor (13). GAPDH was used as an internal control. The primer sequences used in PCR are as follows:

Human NQO1 forward primer: CGCAGACCTTGTGATATTCCAG
Human NQO1 reverse primer: CGTTTCTTCCATCCTTCCAGG
Human HMOX1 forward primer: CTCAAACCTCCAAAAGCC
Human HMOX1 reverse primer: TCAAAAACCACCCCAACC

Human GAPDH forward primer: AAGGTCGGAGTCAACGGA
Human GAPDH reverse primer: CCATGGGTGGAATCATATTGG
Human Nrf2 forward primer: GAGAGCCCAGTCTTCATTGC
Human Nrf2 reverse primer: TGCTCAATGTCCTGTTGCAT

For mouse brains, total RNA was isolated from the frozen cortical tissue using the High Pure RNA Isolation Kit (Roche Life Science, Indianapolis, IN, USA) according to the manufacturer's instructions. RNA concentrations and purity were determined by UV visible absorption spectra, using Nanodrop 2000 (Thermo Fisher Scientific, USA). First-strand cDNA was synthesized with 500ng of total RNA, using iScript cDNA Synthesis Kit (Bio-Rad Laboratories Inc., 1708891, USA) according to the manufacturer's instruction. Quantitative real-time polymerase chain reaction (qRT-PCR) was performed in technical duplicate by using Fast Taqman Master Mix on a QuantStudio™ 6 Pro Real-Time PCR System (Applied Biosystems, USA). Fold change of *Nfe2l2* (Thermo Fisher Scientific, Mm00477784_m1) gene expression was calculated by comparative C_T quantification method and normalized to the expression of internal control gene, *Gapdh* (Thermo Fisher Scientific, Mm99999915_g1).

Silver staining

Free-floating brain sections were washed carefully in 0.1 M phosphate buffer (PB, pH 7.4) and then transferred into 0.1 M PB containing 4% paraformaldehyde for one week. Sections were then processed for the detection of neurodegeneration with the FD NeuroSilverTM Kit II (FD NeuroTechnologies, Columbia, MD; for detailed procedures and references using this product refer to the manual of PK301, available at https://fdneurotech.com). Images were acquired by a Zeiss Axio Imager.M2 microscope using axonal staining to establish the matrices for positive staining and keeping exposure time and light intensity constant. Images were analyzed using the color deconvolution plugin previously described by Ruifrok and Johnston (14) found in ImageJ/Fiji version 2.9.0/1.53T software (NIH, Bethesda, MD). All analysis was conducted blind to genotype.

RNA sequencing

RNA was extracted from frozen cortex tissue of 7-month-old WT, P301S and P301S;*Ssh1*$^{-/-}$ mice using trizol reagent (Ambion, 15596026), and isolated using Monarch Total Miniprep Kit (New England Biolabs, T2021S) following manufacturer's instructions. Sample purity and concentration were determined with Nanodrop One^{C} (Thermo Scientific). Samples were then sent to NovoGene (Beijing, China) for RNA-sequencing as follows.

Degradation and contamination of the RNA was assessed on 1% agarose gel, the purity using the NanoPhotometer® spectrophotometer (IMPLEN, CA, USA), and the integrity and quantity using the RNA Nano 6000 Assay Kit of the Bioanalyzer 2100 system (Agilent Technologies, CA, USA).

mRNA was purified from total RNA with poly-T oligo-attached magnetic beads, and then fragmented using divalent cations under elevated temperature in NEBNext First Strand Synthesis Reaction Buffer (5X). First strand cDNA was synthesized using random hexamer primer and M-MuLV Reverse Transcriptase (RNase H-) and second strand cDNA synthesis was subsequently performed using DNA Polymerase I and RNase H. Remaining overhangs were converted into blunt ends via exonuclease/polymerase activities, and NEBNext Adaptor were ligated to prepare DNA fragments for hybridization after the adenylation of the 3' ends. Library fragments were purified with AMPure XP system (Beckman Coulter, Beverly, USA) to select fragments of 150~200 bp. Then, PCR was performed with Phusion High-Fidelity DNA polymerase, Universal PCR primers and Index (X) Primer. PCR products were purified (AMPure XP system) and library quality was assessed on the Agilent Bioanalyzer 2100 system.

The clustering of the index-coded samples was performed on a cBot Cluster Generation System using PE Cluster Kit cBot-HS (Illumina) following the manufacturer's instructions. After cluster generation, the library preparations were sequenced on an Illumina platform and paired-end reads were generated. Raw reads (FASTQ) were processed through fastp to obtain clean

data by removing reads with adapter and poly-N sequences and low quality. And Q20, Q30 and GC content were calculated.

Reference genome and gene model annotation files were obtained from genome website browser (NCBI/UCSC/Ensembl). Paired-end clean reads were aligned to the reference genome using the Spliced Transcripts Alignment to a Reference (STAR v2.5) software. FeatureCounts was used to count the read numbers mapped of each gene using HTSeq v0.6.1. Then, RPKM of each gene was calculated based on the length of the gene and reads count mapped to this gene.

Qiagen Ingenuity Pathway Analysis (IPA)

Log_2(fold change) of all differentially expressed genes (DEGs) with unadjusted -Log_{10}(*P*-value) of 1.3 were analyzed by Qiagen® Ingenuity pathway analysis (IPA) (Hilden, Germany), a web-based software that includes a database of more than 100,000 curated publicly available datasets to compare and validate. For analysis of canonical or toxicity pathways, the following parameters were chosen: confidence = Experimentally Observed OR High (predicted); tissues/cell lines = all brain cell types and brain-related cell lines; molecule types = all. Activation Z-scores $\geq$2 or $\leq$-2 of canonical pathways are considered significantly activated or inactivated, respectively. The significance in overlap of analysis-ready genes with the total number of genes in the reference canonical or toxicity pathway is expressed by Benjamini-Hochberg adjusted -Log_{10}(*P*-value).

Mouse brain tissue immunohistochemistry (IHC) and Western blotting

Mice were perfused with PBS, and half brains were fixed with 4% paraformaldehyde (PFA) (Acros Organics, 41678-5000) at 4°C for 72 hours followed by cryoprotection in 30% sucrose. After tissue saturation, brains were sliced in 25-µm sections and then processed for IHC staining. Brain sections were washed 3 times with 0.2% triton (Fluka, 93426) in tris-buffered saline (TBS). Tissues were then blocked with 3% normal goat serum (NGS) (Vector Laboratories, S-1000) at room temperature for 1 hour. Indicated primary antibodies were applied overnight at 4°, followed

by secondary antibodies (Alexa Fluor) and DAPI (Thermo Scientific, 62248) incubation at room temperature for 45 min. Tissues were mounted using Fluromount-G (Thermo Fisher Scientific, 00-4958-02).

Each staining procedure included samples processed without primary antibody and only with secondary antibody. Fluorescent images were captured with the Olympus FV10i confocal microscope (Olympus, PA, USA) or Keyence fluorescent microscope BZ-X810 (Keyence, Osaka, Japan). All comparison mages were obtained with the same light intensity, magnification, and exposure time. Fiji Image J software (NIH, https://imagej.net/software/fiji/) was utilized to quantify the immunoreactive signals from images, with background secondary antibody-only signals subtracted. Adjustments to the brightness, contrast, and threshold were applied in the same way in all comparison images, including secondary only controls. Investigators were blinded to genotype during staining, image acquisition, and quantification.

The following antibodies were applied to probe target proteins: rabbit polyclonal anti-Nrf2 (abcam, ab31163); mouse monoclonal anti-8-OHDG (15A3) (Santa Cruz Biotech, sc-66036); rabbit polyclonal anti-Phospho-MAPT/tau (Ser199/202) (Sigma-Aldrich, T6819); rabbit monoclonal anti-β-Amyloid (D54D2) XP® (Cell Signaling Technologies, 8243S); rat monoclonal anti-GFAP (2.2B10) (Invitrogen, 13-0300); rabbit polyclonal anti-Iba1 (Wako Chemicals USA, 019-19741); rabbit monoclonal anti-Synaptophysin (YE269) (abcam, ab32127); Alexa Fluor 594 goat anti-rabbit IgG (Invitrogen, A11037); Alexa Fluor 488 goat anti-rabbit IgG (Invitrogen, A11034); Alexa Fluor 488 goat anti-mouse IgG (Invitrogen, A11029); Alexa Fluor 488 goat anti-rat IgG (Invitrogen, A11006).

For Western blotting, cortical mouse tissues were sonicated in RIPA buffer with protease and phosphatase inhibitors for protein extraction. Samples were centrifuged at 17,000 g for 15 min at 4°C and equalized in concentration using BCA protein assay, and supernatants were used for Western blotting.

Human brain immunohistochemistry and Proximity Ligation Assay (PLA)

For IHC, floating 30-µm paraformaldehyde (PFA)-fixed human brain sections were washed 3 times with 0.2% triton (Fluka, 93426) in tris-buffered saline (TBS). Antigen retrieval was performed by utilizing citrate buffer, pH=6 (Alfa Aesar, J63950) at 95°C for 5 minutes. Tissues were then washed and blocked with 3% normal goat serum (NGS) (Vector Laboratories, S-1000) at room temperature for 1 hour. Indicated primary antibodies were applied overnight at 4°C, followed by secondary antibodies (Alexa Fluor) and DAPI (Thermo Scientific, 62248) for 45 minutes at room temperature. Additionally, TrueBlack® Lipofuscin Autofluorescence Quencher (Biotium, 23007) was used to eliminate autofluorescence and mitigate nonspecific background signals. Each staining procedure included samples processed without primary antibody and only with secondary antibody. Tissues were mounted using Fluromount-G (Thermo Fisher Scientific, 00-4958-02).

For PLA, primary antibodies were followed by the Duolink® In Situ PLA® probes (Sigma-Aldrich, DUO92004 and DUO92002) incubation at 37°C for 1 hour. Duolink® In Situ PLA® ligation and amplification reagents (Sigma-Aldrich, DUO92008 or DUO92013) were incubated at 37°C for 30 min and 100 minutes, respectively, as previously shown (2, 15) before being mounted with the Duolink® In Situ PLA® Mounting Medium with DAPI (Sigma-Aldrich, DUO82040). Each procedure included samples processed with only one primary and only one probe as negative controls. Slides were saved at -20°C. IHC and PLA Images were captured and analyzed in the same way as described for mouse brain tissue.

The following antibodies were used to probe target proteins: rabbit polyclonal anti-SSH1 (ECM Biosciences, SP1711); mouse monoclonal anti-Nrf2 (3G7) (Novus Biologicals, AF4000); rabbit monoclonal anti-Keap1 (D6B12) (Cell Signaling Technologies, 8047); rabbit monoclonal anti-SQSTM1/p62 (D10E10) (Cell Signaling Technologies, 7695); mouse monoclonal anti-Keap1 (1B4) (abcam, ab119403); mouse monoclonal anti-β-Actin (C4) (Santa Cruz Biotech, sc-47778); Alexa Fluor 594 goat anti-rabbit IgG (Invitrogen, A11037); Alexa Fluor 488 goat anti-mouse IgG (Invitrogen, A11029).

Recombinant protein pulldown assay

Final concentrations of 0.5μM His-Nrf2 (MyBiosource, MBS205893) or 0.25μM His-GST-Keap1 (SinoBIological, 11981-H20B) recombinant proteins were incubated with or without 0.2μM GST-SSH1 recombinant protein (Fisher Scientific, 89-963-276) in 1X protein binding buffer (10X: 0.1% triton X-100; 10μM BSA; 200mM Tris-HCl, pH 7.05; 1M KCl, 20mM $MgCl_2$; 2mM ATP; 1mM DTT) for 2 hours at 37°C. After incubation, 1X wash buffer (1% triton X-100; 20mM Tris-HCl, pH 7.05; 100mM KCl; 2mM $MgCl_2$; 100μM DTT) was added to the binding reaction. Samples were pre-cleared with BSA-blocked agarose-bound anti-rabbit beads (American Qualex, G1360B) for 1 hour at 4°C. Following pre-clearing, supernatants were transferred to a new tube containing BSA-blocked agarose-bound anti-rabbit beads (American Qualex, G1360B) and rabbit polyclonal anti-SSH1 antibody (ECM Biosciences, SP1711) (1:100) and allowed to bind at 4°C for 16h. Bound beads were then extensively washed (5x) with 1X wash buffer at room temperature before adding sample buffer and Western blotting. The following antibodies were used to probe target proteins by immunoblotting: Rabbit polyclonal anti-SSH1 (ECM Biosciences, SP1711); rabbit monoclonal anti-Nrf2 (D1Z9C) (Cell Signaling Technologies, 12721); Mouse monoclonal anti-6xHis tag antibody (Thermo Fisher, MA1-21315); peroxidase-Conjugated AffiniPure goat anti-mouse IgG (Jackson ImmunoResearch, 115-035-033); peroxidase-conjugated AffiniPure goat anti-rabbit IgG (Jackson ImmunoResearch, 111-035-033).

Detection of ubiquitinated Nrf2 by immunoprecipitation

HEK293T cells transfected with HA-ubiquitin (Addgene, 18712) were treated $\pm$ 15μM $NaAsO_2$ (18h) and lysed in RIPA buffer (50 mM Tris pH 7.4, 0.1% SDS, 2mM ethylenediaminetetraacetic acid, 150mM NaCl, 1% Triton X-100) with 1% protease inhibitors (GeneDEPOT, P3100-010) and phosphatase inhibitors (GeneDEPOT, P3200-005). Equal protein amounts were then subjected immunoprecipitation for Nrf2 (D1Z9C, Cell Signaling #12721) together with anti-rabbit IgG

agarose (American Qualex, G1360B) overnight at 4°C. Following extensive washing with RIPA buffer, Nrf2 immune complexes were subjected to SDS-PAGE and Western blotting for HA (6E2, Cell Signaling #2367) to detect HA-ubiquitin conjugates. For quantification, ubiquitinated Nrf2 was normalized to Nrf2 pulled down, and statistical analysis was performed by 1-way ANOVA, followed by post hoc Dunnett test and post hoc test for linear trend using GraphPad Prism 8.0.

***Ex vivo* electrophysiological recordings**

Acute hippocampal slices were prepared as previously described (16-19). Briefly, 400μm parasagittal sections were generated in cutting solution using Leica VT1200. Slices were transferred to room temperature cutting solution diluted 1:1 with artificial cerebrospinal fluid (ACSF) (in mM): 125mM NaCl, 2.5mM KCl, 26mM $NaHCO_3$, 1.25mM NaH_2PO_4, 25mM glucose, 1mM $MgCl_2$, and 2mM $CaCl_2$. Slices were maintained in this solution with constant 95% O_2, 5% CO_2 perfusion for 20 min before being transferred to the brain slice recording chamber (BSC1, Scientific Systems Design Inc.).

The recording chamber was held at 30° ± 0.5°C by Proportional Temperature Controller (PTC03, Scientific Systems Design Inc.) with a ACSF flow rate of 1 ml/min. Field excitatory postsynaptic potential (fEPSP) was recorded from stratum radiatum in hippocampal area CA1 via glass electrode (1–4 MΩ) loaded with ACSF. A stimulating electrode made by the formvar-coated nichrome wire (A-M Systems) was positioned on the Schaffer collaterals arising from the CA3 region, which was used to deliver biphasic stimulus pulses (100 μs duration). The electric stimulation, controlled by pClamp 11 software (Molecular Devices), was delivered via the Digidata 1550B interface (Molecular Devices) and a stimulus isolator (model 2200; A-M Systems). The evoked signals were amplified using a differential amplifier (model 1800; A-M Systems), filtered at 10 Hz low cut-off, 20 kHz high cut-off, and digitized at 10 kHz. Input-output (I-O) curves were generated by stepping up stimulation amplitude that elicited half-maximal fEPSP at 0.5mV increments. Paired-pulse facilitation (PPF) was induced with sequential two pulses with interpulse

intervals from 20ms from 20 to 300ms. The percentage of the facilitation was calculated by dividing the fEPSP slope elicited by the second pulse with the fEPSP slope elicited by the first pulse. A 20min baseline fEPSP was recorded at 0.05Hz as a control before the long-term potentiation (LTP). LTP was induced by a high frequency theta burst stimulation (TBS), which consisted of five trains of 200Hz in 20ms duration separated by 200ms, repeated 6 times at 10 s intervals. A 60min fEPSP was recorded at 0.05Hz following TBS. LTP was calculated by dividing the slope of 60 min post-induction responses with the average slope of 20 min baseline responses.

Supplemental Figure Legends

Figure S1 SSH1 inhibits Nrf2/ARE-mediated target gene expression under diverse conditions

(A,C,E) Representative images of HT22 cells co-transfected with the Nrf2 reporter (green & blue) and control siRNA or SSH1 siRNA, treated ± (A) 2 or 8μM $NaAsO_2$ (14h), (C) 2 or 10μM 15d-PGJ2 (14h), or (E) 0.25 or 1μM CDDO-Me (1h), and stained for SSH1 (red). (B,D,F) Quantification of Nrf2/ARE reporter for (B) $NaAsO_2$ (2-way ANOVA, $F(1, 581)=30.37$, $P<0.0001$, post hoc Sidak, ****$P<0.0001$, *$P<0.05$, n = 10-12 images/condition/experiment from 4 experiments), (D) 15d-PGJ2 (2-way ANOVA, $F(1, 574)=87.65$, $P<0.0001$, post hoc Sidak, ****$P<0.0001$, **$P=0.0043$, n = 10-12 images/condition/experiment from 4 experiments), and (F) CDDO-Me (2-way ANOVA, $F(1, 465)=41.66$, $P<0.0001$, post hoc Sidak, ****$P<0.0001$, **$P=0.0067$, *$P=0.0067$, n = 10-12 images/condition/experiment from 4 experiments). (G) Representative immunoblots from HEK293T cell lysates transfected with myc-Nrf2 and vector or Flag-SSH1. (H-J) Quantification of HMOX1, NQO1, and Keap1 proteins (2-tailed *t*-test; HMOX1: $t=4.837$, $df=22$; NQO1: $t=3.099$, $df=18$; Keap1: $t=1.583$, $df=14$; ****$P<0.0001$, **$P<0.01$, ns = not significant, n = 8-10 samples/condition). (K,L) qRT-PCR quantification of HMOX1 and NQO1 mRNA in HEK293T cells transfected with myc-Nrf2 and vector or Flag-SSH1 normalized to Nrf2 and GAPDH mRNA (2-tailed *t*-test; HMOX1: $t=5.541$, $df=34$; NQO1: $t=3.888$, $df=34$; ****$P<0.0001$, ***$P<0.001$, n = 18 samples/condition from 6 experiments).

Figure S2 SSH1-mediated Nrf2 suppression is moderately affected by loss of SQSTM1/p62

(A-C) Representative images of negative controls with only one primary antibody or only one probe for (A) p62-Keap1 PLA, (B) SSH1-p62 PLA, and (C) Keap1-Nrf2 PLA. (D,E) Representative images of HT22 cells transfected with GFP-Nrf2 (green) and vector or Flag-SSH1, showing (D)

p62-Keap1 PLA and (E) Keap1-Nrf2 PLA. (F) Quantification of p62-Keap1 and Keap1-Nrf2 PLA puncta area/cell (2-tailed *t*-test; p62-Keap1 PLA: t=5.439, df=139; Keap1-Nrf2 PLA: t=3.55, df=165; ****P<0.0001, ***P<0.001, n = 15-20 images/condition/experiment from 4 experiments). (G,H) Representative images of negative controls with only 1 primary antibody or only one probe for (G) p62-Keap1 PLA and (H) Keap1-Nrf2 PLA. (I) Representative immunoblots of HA-ubiquitin conjugates in Nrf2 immune complexes from HEK293T cells transfected with HA-ubiquitin ± control siRNA or SSH1 siRNA ± 15μM $NaAsO_2$ treatment (18h). (J) Quantification of Nrf2 ubiquitination normalized to Nrf2 pulldown (1-way ANOVA, F(3, 29)=7.645, P=0.0007, post hoc Dunnett, ***P=0.0004, **P=0.0051; post hoc test for linear trend: dotted line, F(1,29) =22.61, ****P<0.0001; n = 7-9 samples/condition). (K) Representative images of HT22 cells co-transfected with control siRNA or p62 siRNA and vector control or Flag-SSH1 (red), treated ± 8μM $NaAsO_2$ (14h), and stained for Nrf2 (green) and DAPI (blue). (L) Quantification of nuclear Nrf2 intensity (2-way ANOVA, F(1, 631)=240.9, P<0.0001, post hoc Sidak, ****P<0.0001, n = 10-12 images/condition/experiment from 4 experiments). (M) Representative immunoblots of lysates from HT22 cells co-transfected with control siRNA or p62 siRNA and vector control or Flag-SSH1. (N) Representative images of HT22 cells co-transfected with the Nrf2 reporter (green and blue), control siRNA or p62 siRNA, and vector control or Flag-SSH1 (red), treated ± 8μM $NaAsO_2$ (14h), and stained for p62 (magenta) and Flag-SSH1 (red). (O) Quantification of Nrf2 reporter activity (2-way ANOVA, F(1, 629)=258.3, P<0.0001, post hoc Sidak, ****P<0.0001, ***p=0.0002, n = 10-12 images/condition/experiment from 4 experiments).

Figure S3 SSH1 knockdown enhances nuclear Nrf2 levels under diverse Nrf2 activating conditions; and SSH1 catalytic activity is dispensable for Nrf2 sequestration

(A,C,E) Representative images of HT22 cells transfected with control siRNA or SSH1 siRNA, treated ± (A) 2 or 8μM $NaAsO_2$ (14h), (C) 2 or 10μM 15d-PGJ2 (14h), or (E) 0.25 or 1μM CDDO-

Me (1h), and stained for Nrf2 (green), SSH1 (red), and DAPI (blue). (B,D,F) Quantification of nuclear Nrf2 intensity for (B) $NaAsO_2$ (2-way ANOVA, F(1, 856)=38.22, P<0.0001, post hoc Sidak, ****P<0.0001, **P=0.0047, n = 10-12 images/condition/experiment from 4 experiments), (D) 15d-PGJ2 (2-way ANOVA, F(1, 693)=16.60, P<0.0001, post hoc Sidak, ****P<0.0001, **P=0.0036, *P=0.0205, n = 10-12 images/condition/experiment from 4 experiments), and (F) CDDO-Me (2-way ANOVA, F(1, 471)=35.09, P<0.0001, post hoc Sidak, ****P<0.0001, *P=0.0102, n = 10-12 images/condition/experiment from 4 experiments). (G) Representative images of HT22 cells transfected with GFP-Nrf2 (green) and vector or Flag-SSH1 (red). (H) Quantification of nuclear/cytoplasmic GFP-Nrf2 (2-tailed *t*-test, t=5.502, df=152, ****P<0.0001, n = 15-20 images/condition/experiment from 4 experiments). (I) Representative immunoblots of HEK293T cells transfected with vector or myc-Nrf2 and vector, Flag-SSH1, or Flag-SSH1-CS and subjected to cell fractionation for cytosol and cytoskeletal fractions. (J) Quantification of cytoskeletal / cytosolic Nrf2 (1-way ANOVA, F(2, 20) = 7.675, P=0.0034; post hoc Tukey, **P<0.01, *P<0.05, ns= not significant, n= 7-8 samples/condition from 3 experiments). (K) Representative images of negative controls with only one primary or only one probe for SSH1-Nrf2 PLA. (L) Representative images of HT22 cells transfected with GFP (green) and vector, Flag-SSH1, or Flag-SSH1-CS, showing DAPI (blue) and SSH1-Nrf2 PLA (red). (M) Quantification of SSH1-Nrf2 PLA puncta area/cell (1-way ANOVA, F(2, 206)=77.11, P<0.0001; post hoc Tukey, ****P<0.0001, ns=not significant, n = 8-10 images/condition/experiment from 4 experiments).

Figure S4 SSH1-mediated Nrf2 suppression is distinct and separable from SSH1-mediated cofilin activation and p62 autophagy inhibition

(A) Schematic representation of SSH1, SSH1ΔN and SSH1ΔC proteins, showing the phosphatase catalytic domain (CAT) and binding sites for cofilin and p62. (B) Representative images of HT22 cells co-expressing pREP-8xARE-GFP-SV40-BFP Nrf2 reporter (green and blue) with vector, Flag-SSH1, Flag-SSH1ΔN or Flag-SSH1ΔC (red), treated with H_2O_2 (3 h). (C)

Quantification of Nrf2 (1-way ANOVA, F(3, 2551)=33.21, P<0.0001, post hoc Dunnett, ****P<0.0001, **P=0.0018, *P=0.0352, n = 8-12 images/condition/experiment from 4 experiments). (D) Representative immunoblots from HEK293T cells transfected with vector or myc-Nrf2 and vector, Flag-SSH1, Flag-SSH1ΔN, or Flag-SSH1ΔC. (E) Quantification of HMXO1 protein (1-way ANOVA, F(3, 50)=13.06, P<0.0001, post hoc Dunnett, ****P<0.0001, **P=0.0017, *P=0.0315, n = 6-19 samples/condition from 3 experiments). (F) Representative images of HT22 cells transfected with GFP (green) with vector, Flag-SSH1, Flag-SSH1ΔN, or Flag-SSH1ΔC and subjected to PLA for Flag(SSH1)-Nrf2 (red). (G) Quantification of Flag(SSH1)-Nrf2 PLA puncta area/cell (1-way ANOVA, F(2, 265)=31.92, P<0.0001, post hoc Dunnett, ****P<0.0001, n = 10-15 images/condition/experiment from 4 experiments). (H) Representative images of negative controls with only one primary or only one probe for Flag(SSH1)-Nrf2 PLA. (I) Representative immunoblots of HEK293T cells co-expressing myc-Nrf2 with vector, Flag-SSH1, Flag-SSH1ΔN, or Flag-SSH1ΔC, and subjected to cell fractionation for cytosol and cytoskeleton. (J) Quantification of cytoskeletal/cytosolic Nrf2 (1-way ANOVA, F(3, 16)=7.256, P=0.0027, post hoc Dunnett, **P<0.01, *P<0.05, n = 4 samples/condition). (K) Representative images of HT22 cells transfected with GFP-p62-WT or GFP-p62-S349A (green) and vector or Flag-SSH1 and subjected to PLA for p62-Keap1 (red). (L) Representative images of negative controls with only one primary or only one probe for GFP-p62/Keap1 PLA. (M) Quantification of Keap1-p62 PLA area/cell (1-way ANOVA, F(3, 402)=11.45, P<0.0001, post hoc Dunnett, ****P<0.0001, ***P=0.0006, ns=not significant, n = 8-10 images/condition/experiment from 4 experiments). (N) Representative images of HT22 cells transfected with GFP-p62-S403E or GFP-p62-S403A (green) and vector or Flag-SSH1 and subjected to PLA for p62-Keap1 (red). (O) Quantification of p62-Keap1 PLA puncta area/cell (1-way ANOVA, F(3, 334)=36.57, P<0.0001, post hoc Tukey, ****P<0.0001, *P<0.05, n = 8-10 images/condition/experiment from 4 experiments). (P) Representative images of HT22 cells transfected with GFP or GFP-Nrf2 (green) and vector or Flag-SSH1, showing SSH1-Keap1 PLA (red) and F-actin (phalloidin, blue). Negative controls with

only one primary or only one probe are shown below. (Q) Quantification of SSH1-Keap1 PLA puncta intensity/cell (top) and area/cell (bottom) (1-way ANOVA; intensity: $F(2, 154)=71.9$, $P<0.0001$; area: $F(2, 168)=81.52$, $P<0.0001$; post hoc Tukey, **P<0.01, ***P<0.001, ****P<0.0001, n = 10-15 images/condition/experiments from 4 experiments). (R) Quantification of SSH1-Keap1 PLA puncta colocalized with F-actin (top, 1-way ANOVA: $F(2, 187)=26.37$, $P<0.0001$; post hoc Tukey, ****P<0.0001, n = 10-15 images/condition/experiments from 4 experiments) and F-actin colocalized with SSH1-Keap1 PLA puncta (bottom, 1-way ANOVA: $F(2, 188)=26.93$, $P<0.0001$; post hoc Tukey, ****P<0.0001, n = 10-15 images/condition/experiments from 4 experiments). (S) Recombinant His-Nrf2 incubated with recombinant GST-SSH1 for 2h and subjected to IP for SSH1, showing pulldown of His-Nrf2 in the presence of GST-SSH1. Bottom blots show input of GST-SSH1 and His-Nrf2 by straight Western blotting. (T) Quantification of His-Nrf2 pulled down with GST-SSH1 normalized to the no GST-SSH1 condition (2-tailed t-test; $t=2.589$, $df=8$; *P<0.0322, n = 5 samples/condition). (U) Recombinant GST-Keap1 incubated with recombinant GST-SSH1 for 2h and subjected to IP for SSH1, showing nonspecific pulldown of GST-Keap1 in the presence or absence of GST-SSH1. Bottom blots show input of GST-SSH1 and GST-Keap1 by straight Western blotting. (V) Quantification of GST-Keap1 pulled down with GST-SSH1 normalized to the no GST-SSH1 condition (2-tailed t-test; $t=1.744$, $df=8$; n = 5 samples/condition, ns = not significant).

Figure S5 Post-mortem human case information; AD and FTLD-tau brains exhibit disorganization of SSH1 and actin staining

(A) Case information of AD, FTLD-tau, and nondementia control brains. Floating sections of paraformaldehyde-fixed frontal gyrus cortex brain tissues from AD, FTLD-tau, or nondementia control cases were obtained from the Alzheimer's Disease Research Center at Emory University. Available information on APOE genotypes, ethnicity (w=White, b=Black, h=Hispanic), sex (m=male, f=female), post-mortem interval (PMI), age at onset of disease, and age at death are

indicated. (B) Representative images of AD brain negative controls stained with only one primary antibody or only one probe (red) for SSH1-Nrf2 PLA and DAPI (blue). (C) Representative images of nondementia control, FTLD-tau, and AD brain sections stained for SSH1 (red), actin (green), and DAPI (blue). (D) Representative image of AD brain negative control stained with secondary antibody only (red) and DAPI (blue). (E) Representative images of AD brain negative controls stained with only one primary antibody or only one probe (red) for Keap1-Nrf2 PLA and DAPI (blue).

Figure S6 Loss of SSH1 mRNA in *Ssh1*$^{-/-}$ brains

(A) Quantification of SSH1 mRNA by RNA-seq (2-tailed t-test, t=18.09, df=5, ****P<0.0001, n = 3-4 mice/genotype). (B) Representative image of Nrf2 staining negative control stained with secondary antibody only (green) and DAPI (blue) in WT mice. (C) Representative images of 8-OHdG staining negative controls stained with secondary antibody only (green) and DAPI (blue) in WT mice. (D) Representative image of 8-OHdG staining negative control stained with secondary antibody only (red) and DAPI (blue) in APP/PS1 mice. (E) Representative image of Aβ (green) and DAPI (blue) staining in WT mouse cortex.

Figure S7 Input-Output curves in WT, P301S, and P301S;*Ssh1*$^{-/-}$ slices

(A) Input-output (I-O) curves of WT, P301S, and P301S;*Ssh1*$^{-/-}$ brain slices generated by stepping up stimulation amplitude from 1 to 3 mV (n = 14 to 39 slices/genotype from 4 mice/genotype).

Figure S8 Heatmap and canonical pathway analysis of DEGs

(A) Rainbow heatmap comparing Log_2 fold changes of DEGs in P301S mice relative to WT mice and P301S;*Ssh1*$^{-/-}$ mice relative to P301S mice. (B) Qiagen® Ingenuity® pathway analysis (IPA) showing top canonical pathways increased in the cortex of P301S mice compared to WT mice, plotted by Z-score (blue bars) and -Log_{10}(*P*-value) (red circles). Dotted blue line ($\geq$2) = significant

pathway activation Z-score. Dotted red line (≥1.3) = significant adjusted -Log_{10}(*P*-value) for overlap of genes in each pathway. (C) IPA showing top canonical pathways decreased in the cortex of P301S mice compared to WT mice, plotted by negative Z-score (red bars) and -Log_{10}(*P*-value) (blue circles). Dotted red line (≥2) = significant pathway activation Z-score. Dotted blue line (≥1.3) = significant adjusted -Log_{10}(*P*-value) for overlap of genes in each pathway. (D) List of gene IDs and gene symbols overlapping with the Qiagen® IPA canonical Nrf2-mediated oxidative stress response pathway in comparing tau^{P301S};*Ssh1*$^{-/-}$ brains to tau^{P301S} brains with Z-score = 2.23. (E) Graph shows the expression of mouse Nrf2 mRNA normalized to GAPDH mRNA determined by qRT-PCR from RNA isolated from the cortex of 7-month-old WT, tau^{P301S}, and tau^{P301S};*Ssh1*$^{-/-}$ mice (1-way ANOVA, F(2, 22) = 3.995, P=0.0331; post hoc Dunnett, *P=0.0236, n = 6-10 mice/genotype).

Figure S9 Schematic of Nrf2-mediated oxidative stress response in normal and AD brains

In normal brains, SSH1 acts as a molecular 'break' to prevent Nrf2 overactivation under oxidative stress. As transient oxidative stress subsides in a physiological setting, SSH1 activity is suppressed through 14-3-3 binding, which then releases Nrf2 from SSH1, resulting in normal Nrf2-mediated oxidative stress response. By contrast, during AD pathogenesis, constitutively elevated oxidative stress, which activate SSH1 while suppressing Keap1, allow SSH1 to block and override Nrf2-mediated natural neuroprotection by excessively sequestering Nrf2 and indirectly augmenting Keap1-Nrf2 interaction, resulting in exacerbated oxidation, neuroinflammation, autophagy impairment, and proteinopathy.

References

1. S. Kurita, Y. Watanabe, E. Gunji, K. Ohashi, K. Mizuno, Molecular dissection of the mechanisms of substrate recognition and F-actin-mediated activation of cofilin-phosphatase Slingshot-1. *The Journal of biological chemistry* **283**, 32542-32552 (2008).
2. C. Fang *et al.*, SSH1 impedes SQSTM1/p62 flux and MAPT/Tau clearance independent of CFL (cofilin) activation. *Autophagy* **17**, 2144-2165 (2021).
3. Y. Ichimura *et al.*, Phosphorylation of p62 activates the Keap1-Nrf2 pathway during selective autophagy. *Mol Cell* **51**, 618-631 (2013).
4. Y. Katsuragi, Y. Ichimura, M. Komatsu, p62/SQSTM1 functions as a signaling hub and an autophagy adaptor. *The FEBS journal* 10.1111/febs.13540 (2015).
5. G. Matsumoto, T. Shimogori, N. Hattori, N. Nukina, TBK1 controls autophagosomal engulfment of polyubiquitinated mitochondria through p62/SQSTM1 phosphorylation. *Hum Mol Genet* **24**, 4429-4442 (2015).
6. P. Sanchez-Martin, M. Komatsu, p62/SQSTM1 - steering the cell through health and disease. *Journal of cell science* **131** (2018).
7. M. Pilli *et al.*, TBK-1 promotes autophagy-mediated antimicrobial defense by controlling autophagosome maturation. *Immunity* **37**, 223-234 (2012).
8. J. Lim *et al.*, Proteotoxic stress induces phosphorylation of p62/SQSTM1 by ULK1 to regulate selective autophagic clearance of protein aggregates. *PLoS Genet* **11**, e1004987 (2015).
9. Y. Yoshiyama *et al.*, Synapse loss and microglial activation precede tangles in a P301S tauopathy mouse model. *Neuron* **53**, 337-351 (2007).
10. J. L. Jankowsky *et al.*, Mutant presenilins specifically elevate the levels of the 42 residue beta-amyloid peptide in vivo: evidence for augmentation of a 42-specific gamma secretase. *Hum Mol Genet* **13**, 159-170 (2004).
11. H. C. Williams *et al.*, The cofilin phosphatase slingshot homolog 1 restrains angiotensin II-induced vascular hypertrophy and fibrosis in vivo. *Lab Invest* **99**, 399-410 (2019).
12. T. J. Montine *et al.*, National Institute on Aging-Alzheimer's Association guidelines for the neuropathologic assessment of Alzheimer's disease: a practical approach. *Acta Neuropathol* **123**, 1-11 (2012).
13. T. D. Schmittgen, K. J. Livak, Analyzing real-time PCR data by the comparative C(T) method. *Nat Protoc* **3**, 1101-1108 (2008).
14. A. C. Ruifrok, D. A. Johnston, Quantification of histochemical staining by color deconvolution. *Anal Quant Cytol Histol* **23**, 291-299 (2001).
15. J. A. Woo *et al.*, Activated cofilin exacerbates tau pathology by impairing tau-mediated microtubule dynamics. *Commun Biol* **2**, 112 (2019).
16. J. A. Woo *et al.*, Slingshot-Cofilin activation mediates mitochondrial and synaptic dysfunction via Abeta ligation to beta1-integrin conformers. *Cell Death Differ* **22**, 921-934 (2015).
17. Y. Yan *et al.*, X-linked ubiquitin-specific peptidase 11 increases tauopathy vulnerability in women. *Cell* 10.1016/j.cell.2022.09.002 (2022).
18. T. Liu *et al.*, Modulation of synaptic plasticity, motor unit physiology, and TDP-43 pathology by CHCHD10. *Acta Neuropathol Commun* **10**, 95 (2022).
19. J. A. Woo *et al.*, beta-Arrestin2 oligomers impair the clearance of pathological tau and increase tau aggregates. *Proc Natl Acad Sci U S A* **117**, 5006-5015 (2020).

Figure S1

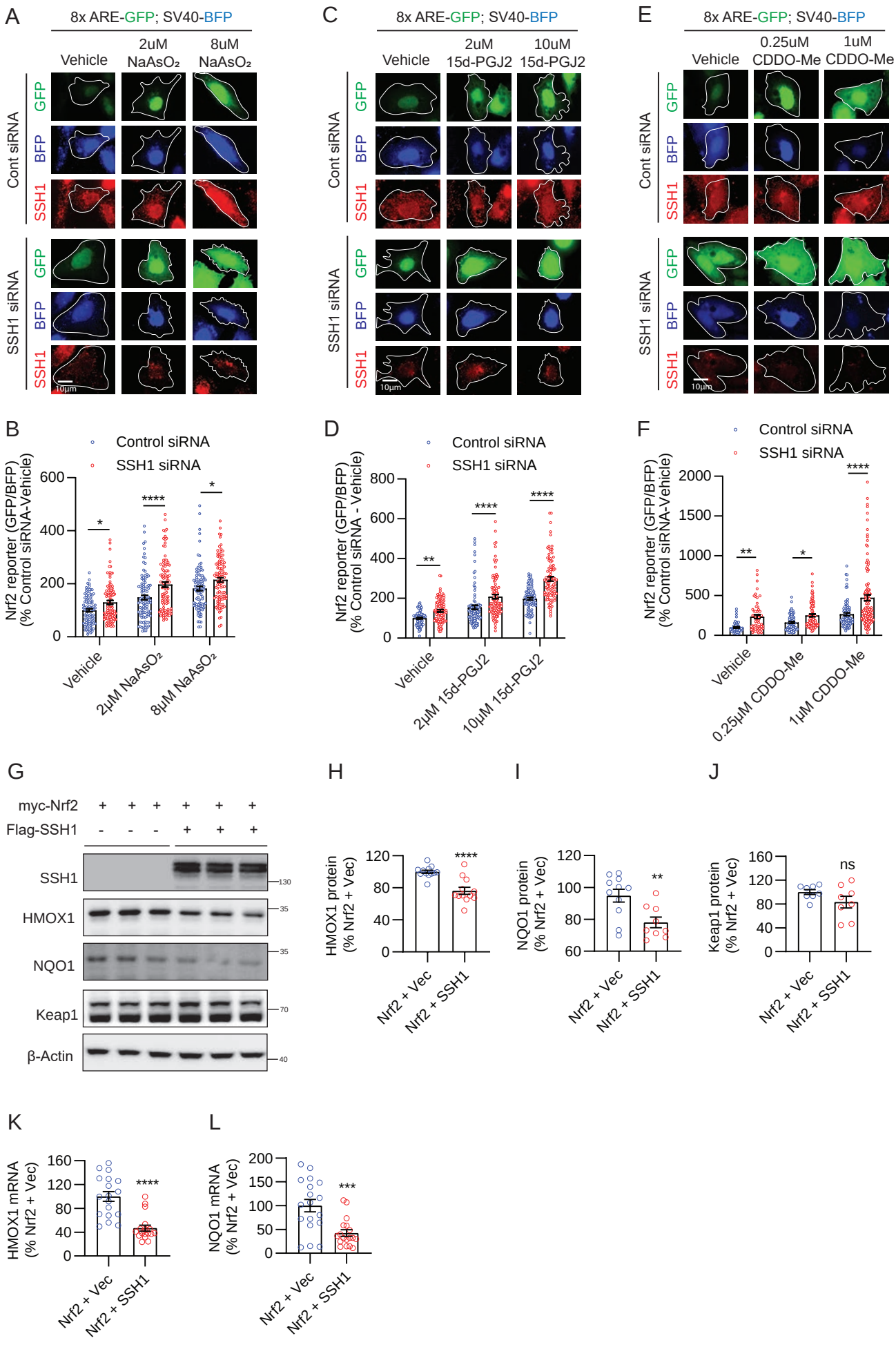
A
8x ARE-GFP; SV40-BFP
Vehicle
2uM NaAsO2
8uM NaAsO2
Cont siRNA
SSH1 siRNA
GFP
BFP
SSH1
10μm
B
Control siRNA
SSH1 siRNA
Nrf2 reporter (GFP/BFP) (% Control siRNA-Vehicle)
Vehicle
2μM NaAsO2
8μM NaAsO2
C
8x ARE-GFP; SV40-BFP
Vehicle
2uM 15d-PGJ2
10uM 15d-PGJ2
D
Control siRNA
SSH1 siRNA
Nrf2 reporter (GFP/BFP) (% Control siRNA - Vehicle)
Vehicle
2μM 15d-PGJ2
10μM 15d-PGJ2
E
8x ARE-GFP; SV40-BFP
Vehicle
0.25uM CDDO-Me
1uM CDDO-Me
F
Control siRNA
SSH1 siRNA
Nrf2 reporter (GFP/BFP) (% Control siRNA-Vehicle)
Vehicle
0.25μM CDDO-Me
1μM CDDO-Me
G
myc-Nrf2
Flag-SSH1
SSH1
HMOX1
NQO1
Keap1
β-Actin
H
HMOX1 protein (% Nrf2 + Vec)
Nrf2 + Vec
Nrf2 + SSH1
I
NQO1 protein (% Nrf2 + Vec)
Nrf2 + Vec
Nrf2 + SSH1
J
Keap1 protein (% Nrf2 + Vec)
ns
Nrf2 + Vec
Nrf2 + SSH1
K
HMOX1 mRNA (% Nrf2 + Vec)
Nrf2 + Vec
Nrf2 + SSH1
L
NQO1 mRNA (% Nrf2 + Vec)
Nrf2 + Vec
Nrf2 + SSH1

Figure S2

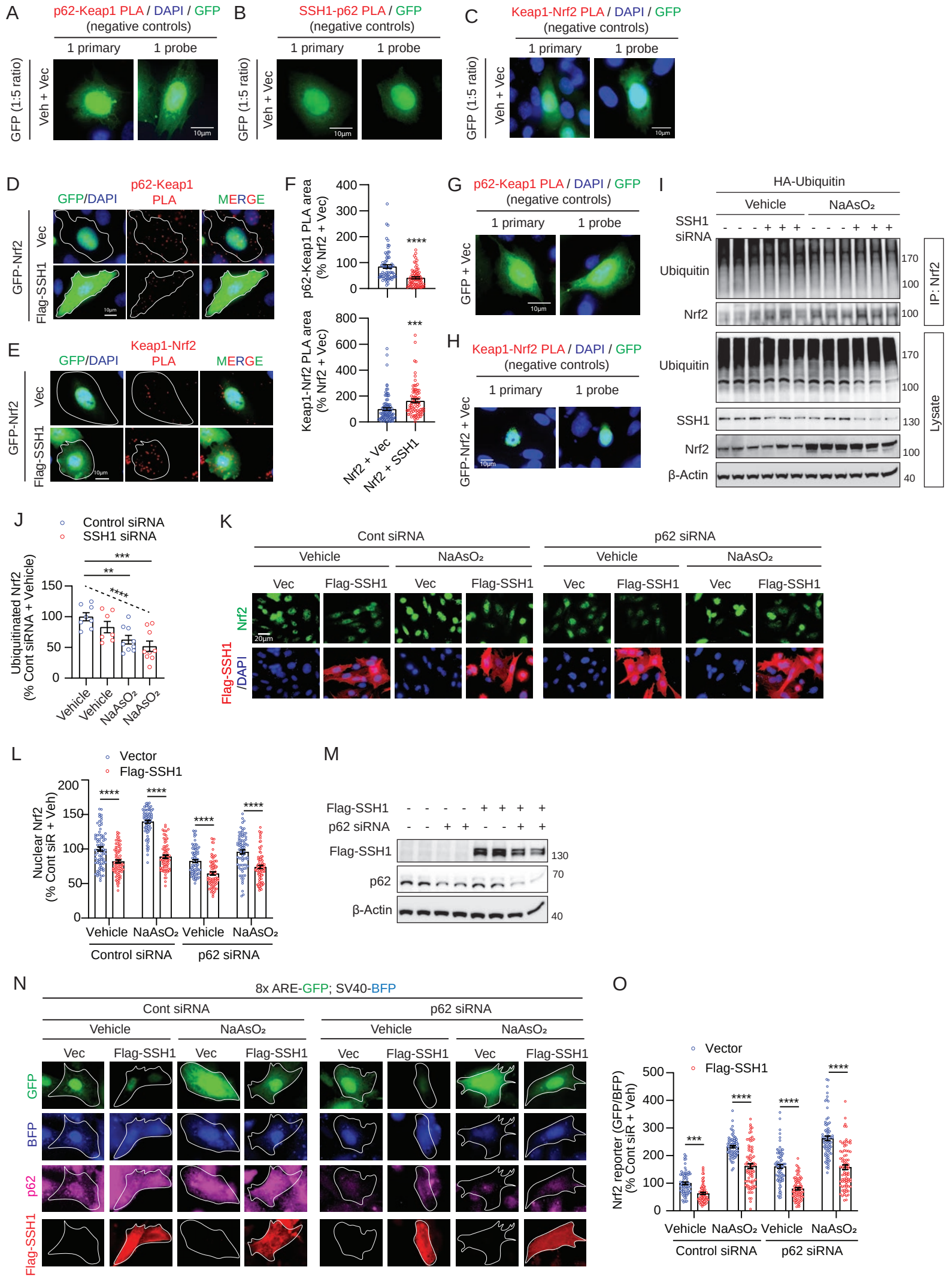
A
p62-Keap1 PLA / DAPI / GFP
(negative controls)
1 primary
1 probe
GFP (1:5 ratio)
Veh + Vec
10μm
B
SSH1-p62 PLA / GFP
(negative controls)
C
Keap1-Nrf2 PLA / DAPI / GFP
(negative controls)
D
GFP/DAPI
p62-Keap1 PLA
MERGE
GFP-Nrf2
Vec
Flag-SSH1
E
Keap1-Nrf2 PLA
F
p62-Keap1 PLA area (% Nrf2 + Vec)
Keap1-Nrf2 PLA area (% Nrf2 + Vec)
****
***
Nrf2 + Vec
Nrf2 + SSH1
G
H
GFP-Nrf2 + Vec
I
HA-Ubiquitin
Vehicle
NaAsO₂
SSH1 siRNA
Ubiquitin
Nrf2
SSH1
β-Actin
IP: Nrf2
Lysate
J
Control siRNA
SSH1 siRNA
Ubiquitinated Nrf2 (% Cont siRNA + Vehicle)
K
Cont siRNA
p62 siRNA
Nrf2
Flag-SSH1 /DAPI
20μm
L
Vector
Flag-SSH1
Nuclear Nrf2 (% Cont siR + Veh)
Control siRNA
p62 siRNA
M
p62
N
8x ARE-GFP; SV40-BFP
GFP
BFP
p62
O
Nrf2 reporter (GFP/BFP) (% Cont siR + Veh)

Figure S3

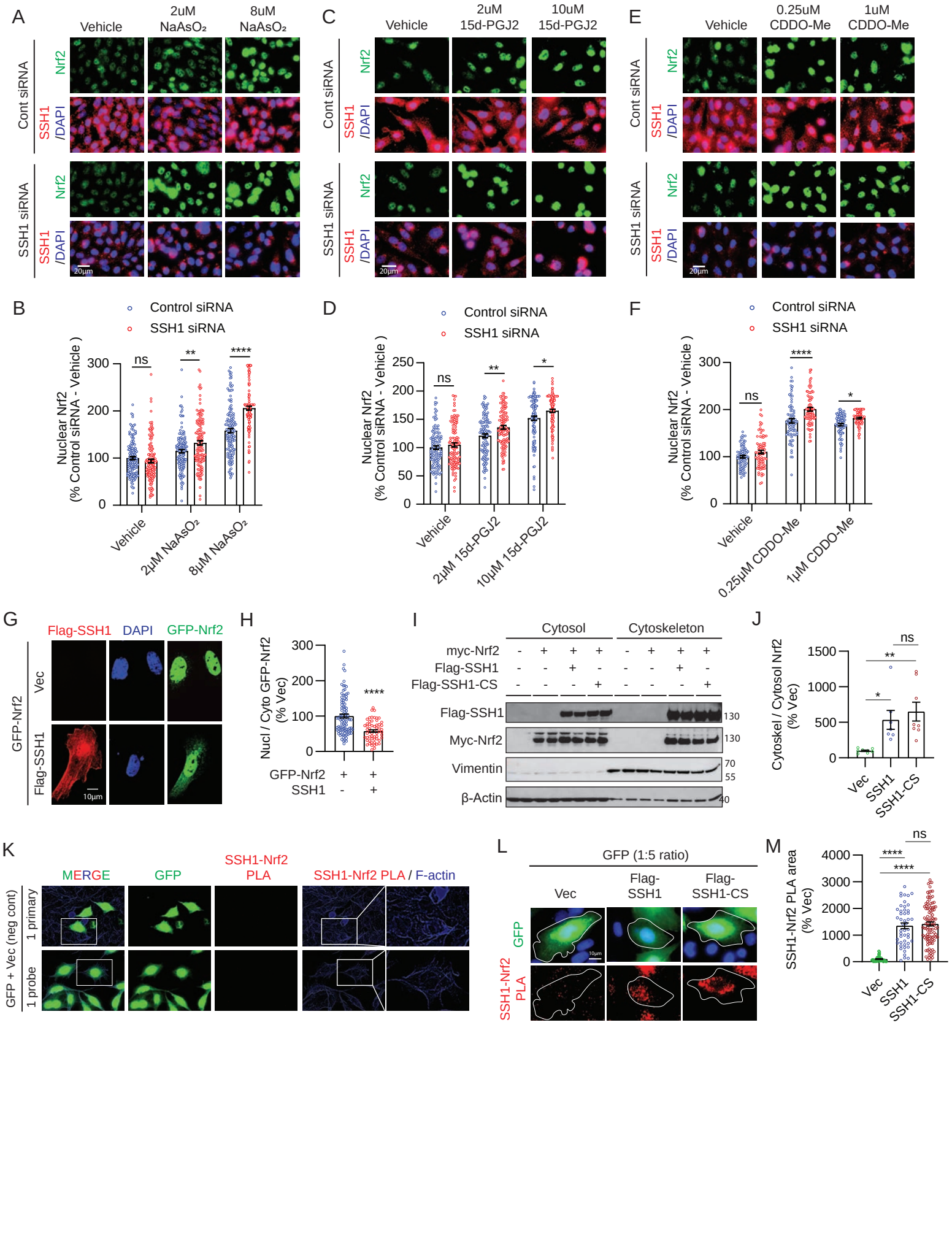
A
Vehicle
2uM NaAsO₂
8uM NaAsO₂
Cont siRNA
SSH1 siRNA
Nrf2
SSH1 /DAPI
20μm
C
Vehicle
2uM 15d-PGJ2
10uM 15d-PGJ2
E
Vehicle
0.25uM CDDO-Me
1uM CDDO-Me
B
Control siRNA
SSH1 siRNA
Nuclear Nrf2 (% Control siRNA - Vehicle)
ns
**
****
Vehicle
2μM NaAsO₂
8μM NaAsO₂
D
*
2μM 15d-PGJ2
10μM 15d-PGJ2
F
0.25μM CDDO-Me
1μM CDDO-Me
G
Flag-SSH1
DAPI
GFP-Nrf2
Vec
Flag-SSH1
10μm
H
Nucl / Cyto GFP-Nrf2 (% Vec)
GFP-Nrf2
SSH1
I
Cytosol
Cytoskeleton
myc-Nrf2
Flag-SSH1
Flag-SSH1-CS
Vimentin
β-Actin
J
Cytoskel / Cytosol Nrf2 (% Vec)
Vec
SSH1
SSH1-CS
K
MERGE
GFP
SSH1-Nrf2 PLA
SSH1-Nrf2 PLA / F-actin
GFP + Vec (neg cont)
1 primary
1 probe
L
GFP (1:5 ratio)
Vec
Flag-SSH1
Flag-SSH1-CS
GFP
SSH1-Nrf2 PLA
M
SSH1-Nrf2 PLA area (% Vec)

Figure S4

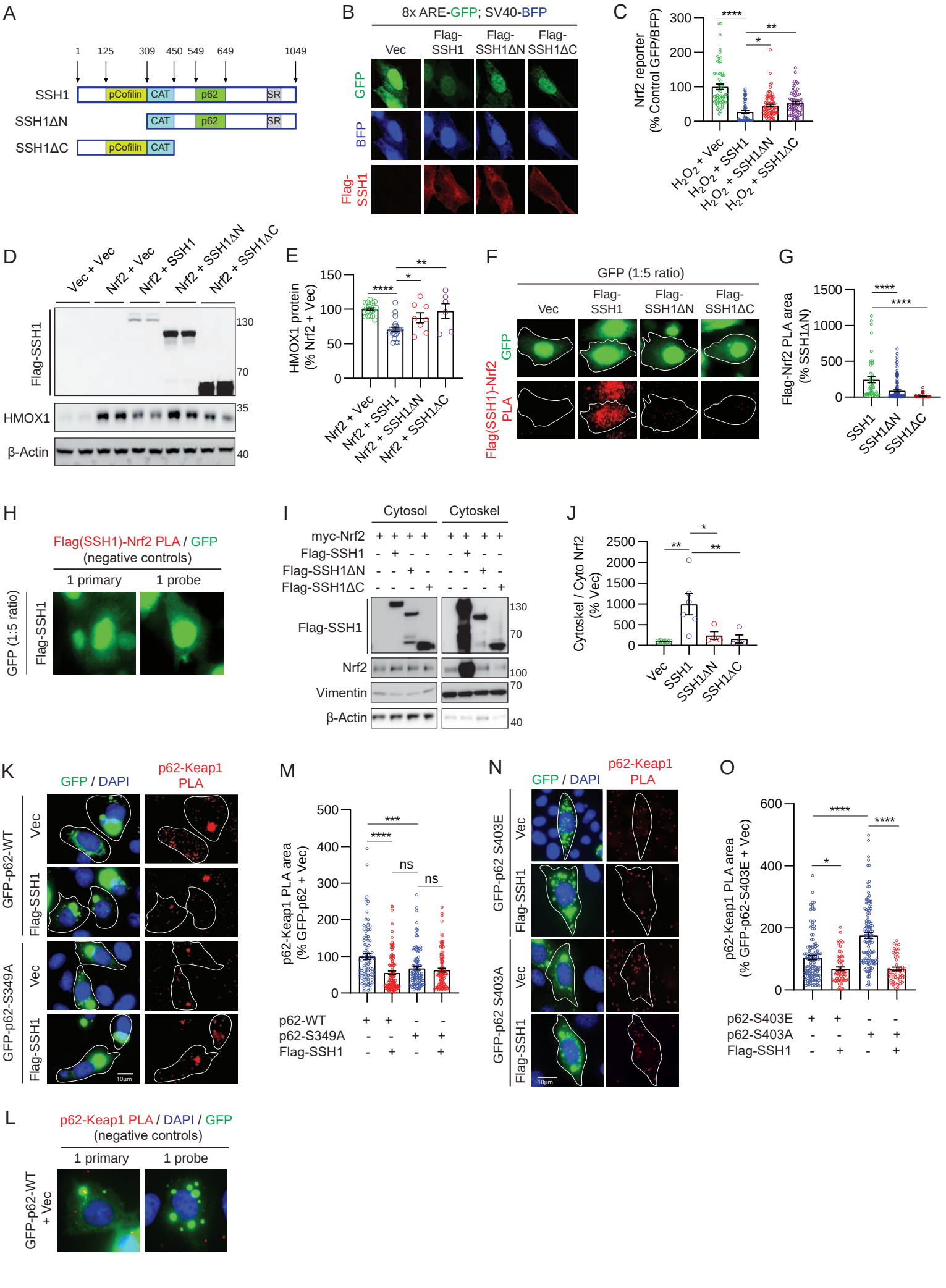
A
1
125
309
450
549
649
1049
SSH1
pCofilin
CAT
p62
SR
SSH1ΔN
SSH1ΔC
B
8x ARE-GFP; SV40-BFP
Vec
Flag-SSH1
Flag-SSH1ΔN
Flag-SSH1ΔC
GFP
BFP
Flag-SSH1
C
Nrf2 reporter (% Control GFP/BFP)
H2O2 + Vec
H2O2 + SSH1
H2O2 + SSH1ΔN
H2O2 + SSH1ΔC
D
Vec + Vec
Nrf2 + Vec
Nrf2 + SSH1
Nrf2 + SSH1ΔN
Nrf2 + SSH1ΔC
Flag-SSH1
HMOX1
β-Actin
E
HMOX1 protein (% Nrf2 + Vec)
F
GFP (1:5 ratio)
Flag(SSH1)-Nrf2 PLA
G
Flag-Nrf2 PLA area (% SSH1ΔN)
H
Flag(SSH1)-Nrf2 PLA / GFP (negative controls)
1 primary
1 probe
GFP (1:5 ratio)
I
Cytosol
Cytoskel
myc-Nrf2
Flag-SSH1
Flag-SSH1ΔN
Flag-SSH1ΔC
Nrf2
Vimentin
J
Cytoskel / Cyto Nrf2 (% Vec)
K
GFP / DAPI
p62-Keap1 PLA
GFP-p62-WT
GFP-p62-S349A
M
p62-Keap1 PLA area (% GFP-p62 + Vec)
p62-WT
p62-S349A
N
GFP-p62 S403E
GFP-p62 S403A
O
p62-Keap1 PLA area (% GFP-p62-S403E + Vec)
p62-S403E
p62-S403A
L
p62-Keap1 PLA / DAPI / GFP (negative controls)

Figure S4 continued

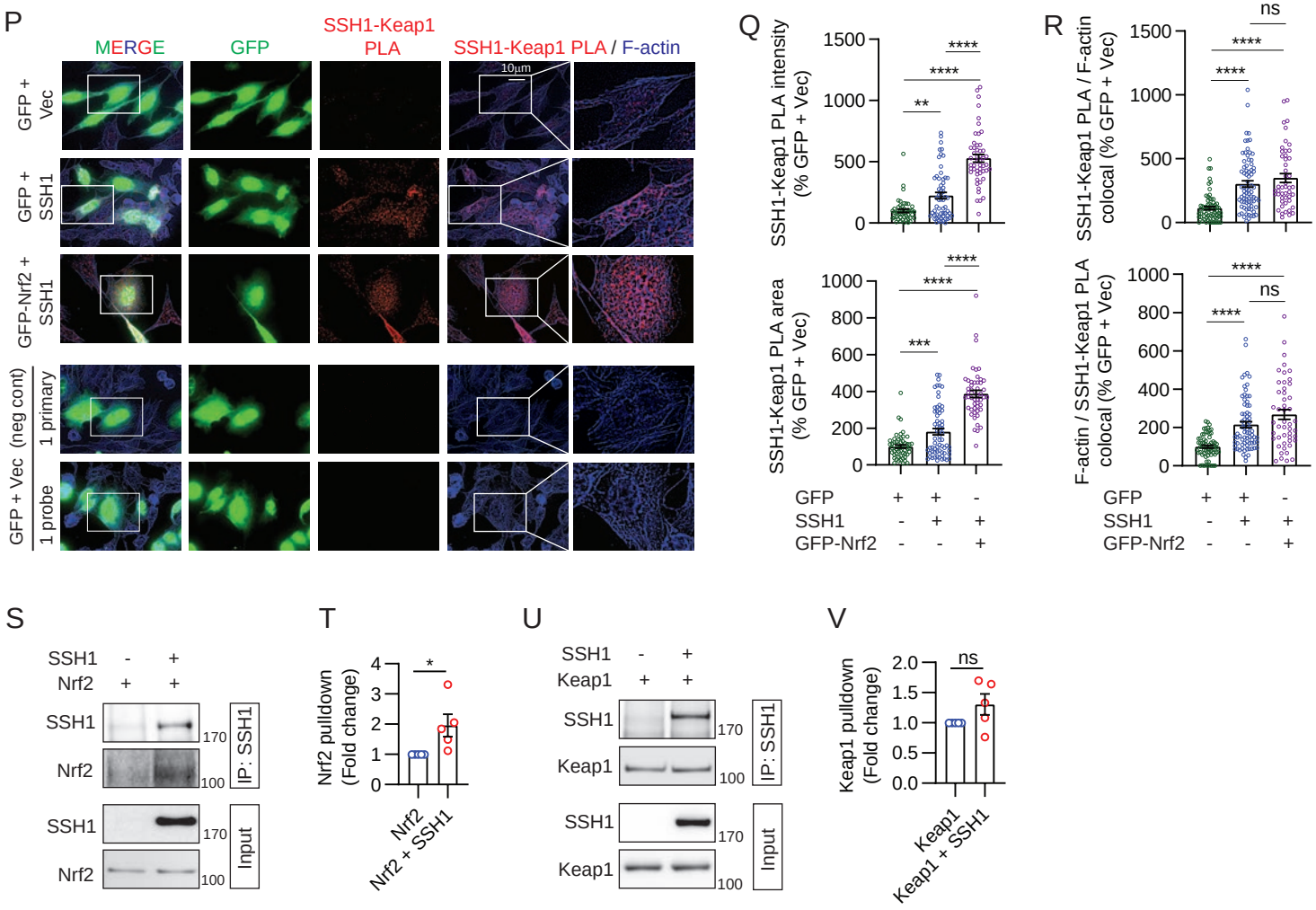

Figure S5

A

Case Number	Primary Neuropathologic Diagnosis	PMI (hr)	Age at Onset	Age at Death	Duration	ApoE	Race/Sex
OS99-08	Control	3		74		E3/3	wf
OS00-23	Control	11		68		E3/3	bf
OS02-35	Control	6		75		E3/3	wf
OS03-299	Control	6		69		E3/3	wm
OS03-390	Control	7		74		E3/3	wf
E04-34	Control	17		57		E3/3	bf
E05-74	Control	6		59		E2/3	bm
E10-142	Control	5.5		94		E3/3	wm
E04-186	AD	7	59	72	13	E3/4	wf
E05-04	AD	4.5	52	64	12	E3/4	wf
E05-90	AD	8	69	76	7	E3/4	wf
E05-194	AD	15	69	71	2.5	E3/4	wm
E06-155	AD	6.5	56	67	11	E2/3	wm
E07-36	AD	22		91		E3/3	wm
E12-06	AD	14.5	60	68	8	E3/3	wm
OS00-13	FTLD-tau (CBD)	5	57	62	5	E3/3	wm
OS00-39	FTLD-tau (CBD)	2.75	56	61	5	E2/3	hm
OS02-73	FTLD-tau (CBD)	24	33	44	11	E3/4	wm
E07-70	FTLD-tau (Pick's)	4	65	81	16	E3/3	wm
E14-123	FTLD-tau (Pick's)	17	58	71	13		wm
E15-66	FTDP-17 (P301L)	34.5	51	56	5		wf
OS-150716	FTDP-17 (R406W)	15		65			wf
E17-22	FTDP-17 (G389R)	18.5	36	40	4		wm

B

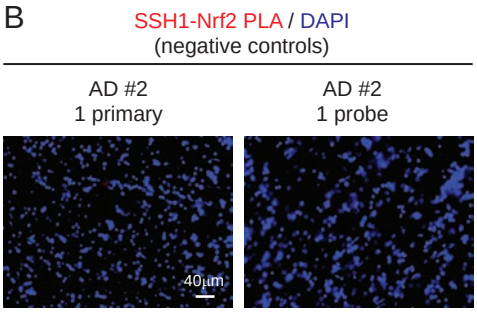

C

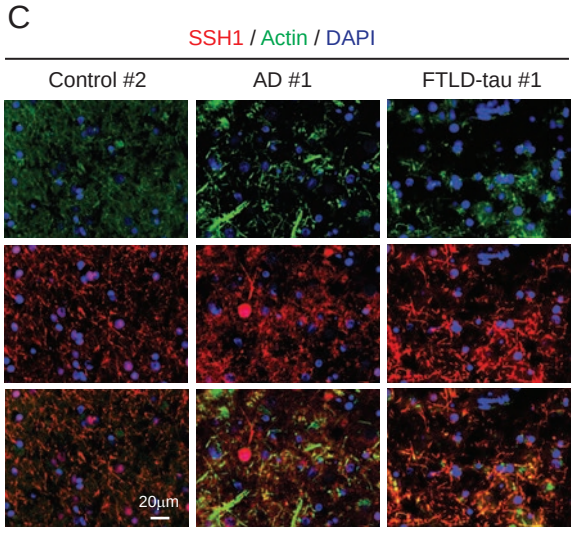

D

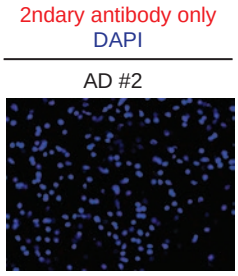

E

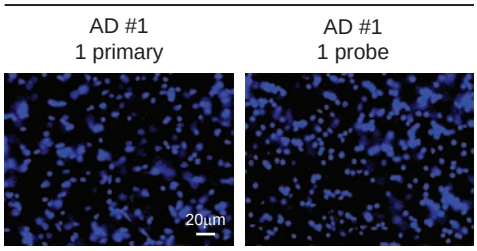

Figure S6

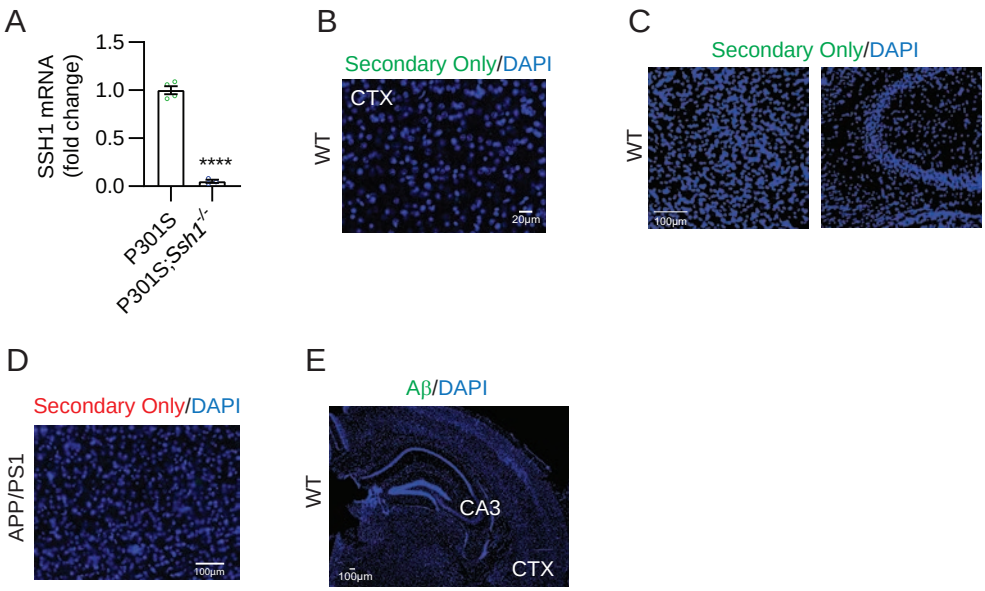
A
SSH1 mRNA (fold change)
1.5
1.0
0.5
0.0
****
P301S
P301S;Ssh1-/-
B
Secondary Only/DAPI
WT
CTX
20μm
C
Secondary Only/DAPI
WT
100μm
D
Secondary Only/DAPI
APP/PS1
100μm
E
Aβ/DAPI
WT
CA3
CTX
100μm

Figure S7

A

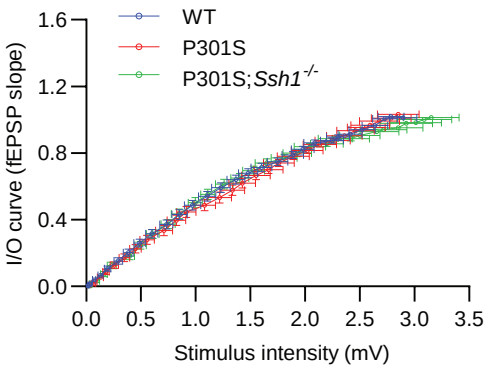
WT
P301S
P301S;Ssh1-/-
I/O curve (fEPSP slope)
1.6
1.2
0.8
0.4
0.0
0.0
0.5
1.0
1.5
2.0
2.5
3.0
3.5
Stimulus intensity (mV)

Figure S8

A

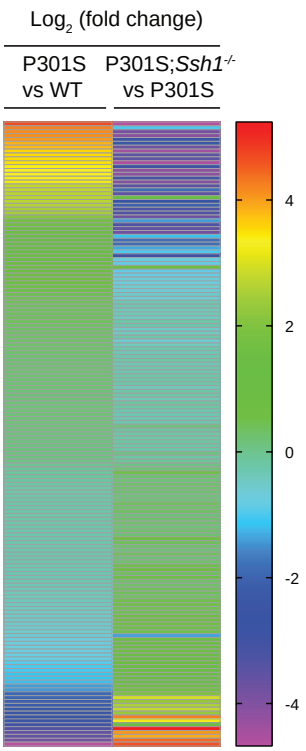

B

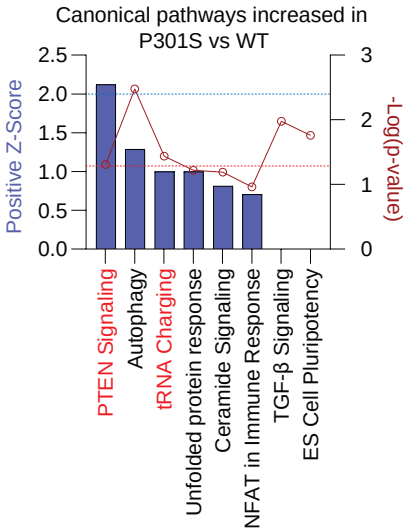

C

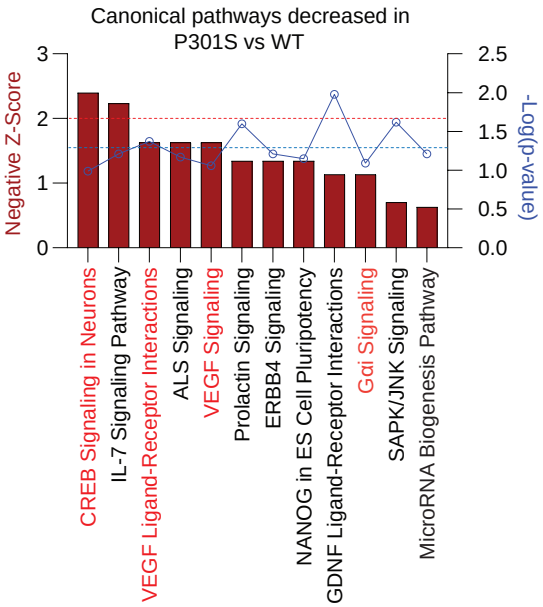

D

Nrf2-mediated Oxidative Stress Response	
gene_id	gene_name
ENSMUSG00000032849	Abcc4
ENSMUSG00000030670	Cyp2r1
ENSMUSG00000026740	Dnajc1
ENSMUSG00000036764	Dnajc12
ENSMUSG00000024963	Dnajc4
ENSMUSG00000055024	Ep300
ENSMUSG00000041548	Hspb8
ENSMUSG00000026688	Mgst3
ENSMUSG00000032470	Mras
ENSMUSG00000003849	Nqo1
ENSMUSG00000030660	Pik3c2a
ENSMUSG00000052889	Prkcb
ENSMUSG00000029053	Prkcz
ENSMUSG00000027011	Ube2e3

E

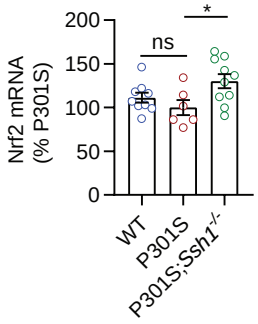

Figure S9

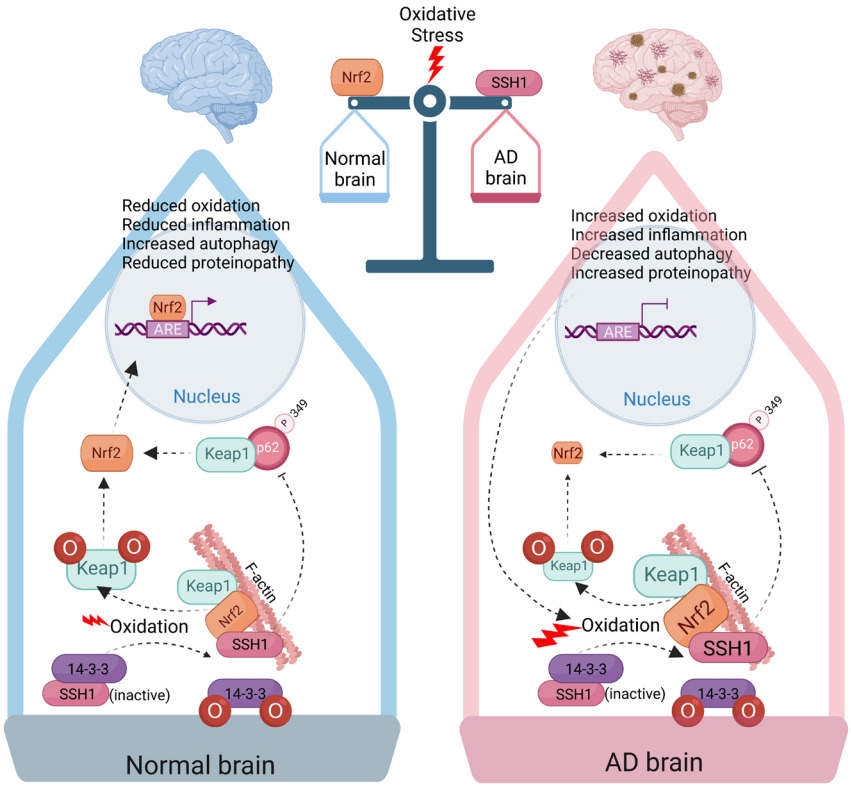
Oxidative Stress
Nrf2
SSH1
Normal brain
AD brain
Reduced oxidation
Reduced inflammation
Increased autophagy
Reduced proteinopathy
Nrf2
ARE
Nucleus
Nrf2
Keap1
p62
P 349
Keap1
Keap1
F-actin
Nrf2
Oxidation
SSH1
14-3-3
SSH1 (inactive)
14-3-3
Normal brain
Increased oxidation
Increased inflammation
Decreased autophagy
Increased proteinopathy
ARE
Nucleus
Nrf2
Keap1
p62
P 349
Keap1
Keap1
F-actin
Nrf2
Oxidation
SSH1
14-3-3
SSH1 (inactive)
14-3-3
AD brain